Synthesis and Luminescence Properties of Near-Infrared N-Heterocyclic Luciferin Analogues for In Vivo Optical Imaging

doi: 10.1246/bcsj.20180350

Synthesis and luminescence properties of near-infrared *N*-heterocyclic luciferin analogues for *in vivo* optical imaging

Ryohei Saito,[1, 2] Takahiro Kuchimaru,[3, 4] Shoko Higashi,[1, 5] Shijia W. Lu,[1, 6] Masahiro Kiyama,[1] Satoshi Iwano,[1, 7] Rika Obata,[8] Takashi Hirano,[1] Shinae Kizaka-Kondoh,*[3] and Shojiro A. Maki*[1, 2]

[1] Department of Engineering Science, Graduate School of Informatics and Engineering, The University of Electro-Communications, 1-5-1 Chofugaoka, Chofu, Tokyo, 182-8585, Japan

[2] Brain Science Inspired Life Support Research Center, The University of Electro-Communications, 1-5-1 Chofugaoka, Chofu, Tokyo, 182-8585, Japan

[3] School of Life Science and Technology, Tokyo Institute of Technology, 4259 Nagatsuta, Midori-ku, Yokohama, Kanagawa, 226-8501, Japan

[4] (Current) Center for Molecular Medicine, Jichi Medical University, 3311-1 Yakushiji, Shimotsuke, Tochigi, 329-0498, Japan

[5] (Current) Department of Chemistry, Faculty of Science, Toho University, 2-2-1 Miyama, Funabashi, Chiba, 274-8510, Japan

[6] (Current) Sydney Medical Program, University of Sydney, Edward Ford Building A27, Camperdown, NSW, 2006, Australia

[7] (Current) Laboratory for Cell Function and Dynamics, Center for Brain Science, RIKEN, 2-1 Hirosawa, Wako, Saitama, 351-0198, Japan

[8] Research and Education Center for Natural Sciences, Keio University, 4-1-1 Hiyoshi, Kohoku-ku, Yokohama, Kanagawa, 223-8521, Japan

E-mail: s-maki@uec.ac.jp (S. A. Maki), skondoh@bio.titech.ac.jp (S. K-Kondoh)

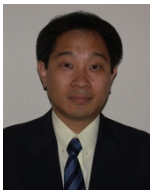

Shojiro A. Maki is an Associate Professor of the Department of Engineering Science, The University of Electro-Communications (UEC). He received his Ph.D. from KEIO University in 1994. He served as an Assistant Professor in the Department of Applied Physics and Chemistry, the University of Electro-Communications from 1996 to 2018. He won the Koizumi Memorial Fellowship Award, KEIO University in 1990, the Incentive Award for Organic Electron Transfer Chemistry in 2005, and the "The best Teacher Award", The University of Electro-Communications in 2012. He was a member of the "Road mapping Converging Technologies to Combat Emerging Infectious Diseases" on APEC Center for Technology Foresight.

Shinae Kizaka-Kondoh is a professor of the School of Life Science and Technology, Tokyo Institute of Technology. She received her Ph.D. from the Graduate School of Medicine, Osaka University in 1989. She became an Assistant Professor in the Graduate School of Medicine at Kyoto University in 1999, Associate Professor in 2004, and Professor in 2008. She has been a full professor at Tokyo Institute of Technology since 2010. Her research interest include in vivo optical imaging technique, and drug development to target tumor microenvironment such as hypoxia and immunosuppression.

Abstract

As a means to achieving highly sensitive bioluminescence imaging of deep tissues utilizing the firefly luciferin-luciferase (L-L) reaction, we previously reported a luciferin analogue, AkaLumine, which exhibits high cell-permeability and emits near-infrared (NIR) light with high tissue-penetration by the L-L reaction. However, while AkaLumine enables us to observe targets in deep tissues, its poor solubility in aqueous media limits its utility for *in vivo* imaging. Herein, to address this issue, we have synthesized three AkaLumine derivatives with *N*-heterocyclic aromatic rings as new red luciferin analogues that have substantially higher solubility than that of AkaLumine in phosphate buffered saline solution. One of the derivatives (herein termed seMpai) exhibits an emission maximum at 675 nm upon L-L reaction with *Photinus pyralis* luciferase and presents an activity in mouse-tissue imaging similar to that of AkaLumine. It is hoped that seMpai will extend the application of high-sensitivity NIR bioluminescence imaging in a wide range of biomedical research fields.

Keywords: Bioluminescence, NIR, Deep tissue imaging

1. Introduction

In terms of biological and medical research, *in vivo* optical imaging plays a vital role in the study of biological processes in living cells and organs.[1,2,3] Firefly bioluminescence is one of the most commonly used light sources for fast, safe, and non-invasive *in vivo* optical imaging.[4,5] Firefly bioluminescence is based on the enzymatic reaction of the

substrate firefly luciferin (LH_2, Scheme 1) with ATP, Mg^{2+} and O_2 in the presence of the firefly luciferase (FLuc). This is termed the luciferin-luciferase (L-L) reaction, and it results in a yellow-green light emission (bioluminescence emission maximum (λ_{BL}): 560 nm).[6,7] Bioluminescence imaging (BLI) using the L-L reaction is performed using a simple instrument comprising a photon detector in a dark box. Because the technique, unlike fluorescence measurement, does not rely on an external light source for excitation, there are no negative effects due to the scattering of excitation light. In addition, auto-luminescence signals generated by LH_2 in living tissues are extremely low.[8] Thus, BLI provides imaging data with a low signal-to-noise ratio.

In the L-L reaction for BLI, the combination of LH_2 and FLuc provides highly efficient light emission. However, the yellow-green light emitted by the L-L reaction of LH_2 with FLuc is largely absorbed and easily scattered by biological tissues.[9,10] To achieve *in vivo* optical imaging with good penetration to deep biological tissues, L-L reactions that produce light in the near-infrared (NIR) range (650–900 nm), termed the optical window, are required. To obtain NIR light by L-L reactions, improved luciferin analogues and mutant luciferases have been developed.[11,12,13] Luciferin analogues containing fused azacycles[4] or with conjugated NIR fluorophores[14] have been developed. Also, Hall et al reported NIR (730 and 743 nm) bioluminescence imaging which is the combination of the modified naphthyl analogues and the mutant luciferase.[15] Our group has developed NIR luciferin analogues with phenylbutadienyl and biphenyl moieties by modification of the π-electronic conjugated structure of LH_2.[16,17] The phenylbutadienyl analogue AkaLumine (**1a**, Scheme 1) shows improved bioluminescence activity with FLuc. In order to further tune and improve the luminescence properties of **1a**, cyclic amino analogues[18] and allyl-substituted[19] analogues of **1a** have also been developed. The λ_{BL} of **1a** with FLuc is observed at 675 nm,[16] leading to more sensitive detection in deep tissues than that achieved with LH_2.[20] However, although **1a** represents a breakthrough in the development of compounds for deep tissue *in vivo* optical imaging research, it exhibits problematically poor water solubility. In fact, the solubility of **1a** in phosphate buffered saline (PBS) is lower than that of LH_2. Thus, in order to expand the utility of **1a** and its analogues,[20] it is necessary to improve their water solubilities. One of the possible methods to solve this problem is to prepare a salt of **1a** with an acid. Accordingly, the hydrochloride salt of **1a**, termed TokeOni (**1a**-HCl) was found to exhibit good water solubility (30–100 mM in water)[20,21] and enables the detection of deep targets in the brain of mice and marmosets when reacted with mutant luciferase AkaLuc, which is specifically optimized for the L-L reaction with **1a**-HCl.[21] As another approach, we planned to introduce a hydrophilic moiety into the structure of **1a**. Because *N*-heterocycles such as pyridine and pyrazine have water solubilities that are generally higher than that of benzene,[22] we designed the *N*-aryl analogues **1b–d** (Scheme 1). Since **1b–d** are bioisosteres of **1a**, they were reasonably expected to act effectively as substrates of firefly luciferase. Herein, we report the syntheses, water solubilities, and luminescence properties of **1b–d**. Of these analogues, **1c** shows a bioluminescence activity similar to that of **1a**. We also investigated cellular and animal imaging with **1c** together with LH_2 and **1a**-HCl.

2. Experimental

2.1. General. Commercially available reagents and solvents were used without further purification. AkaLumine (**1a**) and TokeOni (**1a**-HCl) were provided by Kurogane Kasei Co., Ltd., for bioluminescence measurements, and recombinant *Ppy* luciferase (QuantiLum® recombinant luciferase, E1701, Promega) was used. Wako Silica gel 70 F254 TLC plates were used for analytical TLC, and Kanto Chemical Silica gel 60 N (spherical, neutral) were used for column chromatography. For preparative flash chromatography, an automated system (Smart Flash EPCLC AI-580S, Yamazen Corp., Japan) were used with universal columns of silica gel. Melting points were measured with a Yanaco MP-500P. IR spectra were obtained with a Nicolet 6700 spectrometer with an ATR attachment. ^1H and ^{13}C NMR spectra were recorded on a JEOL ECA-500 instrument (500 MHz for ^1H and 126 MHz for ^{13}C). High-resolution electro-spray ionization mass spectra were obtained with a JEOL JMS-T100LC mass spectrometer. The optical purities of *N*-Aryl analogues were analyzed by Daicel's chiral columns screening service (Daicel Chemical Industries, CHIRALPAK® IG, 5 μm, 4.6 mm × 150 mm, flow rate 0.8 mL/min). UV/visible absorption spectra were obtained using an Agilent Technologies Cary 60 spectrophotometer (scan speed 600 nm/min; data interval 1 nm). Bioluminescence and chemiluminescence spectra were measured with an ATTO AB-1850 spectrophotometer (data interval 1 nm). Bioluminescence intensities were monitored using an ATTO AB-2270 and a Microtec Co. GL-201A luminometer. Density functional theory (DFT) calculations were performed with the Gaussian 09 program (Rev. D.01).[23] DFT included the B3LYP function with the 6-31+G(d) basis set.[24,25,26] Molecular graphics were prepared with GaussView, Version 5.[27] BLI was performed with a multifunctional *in vivo* imaging system (IVIS Spectrum, PerkinElmer).

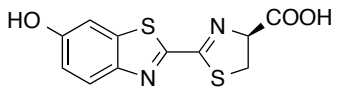

Firefly luciferin (LH_2)

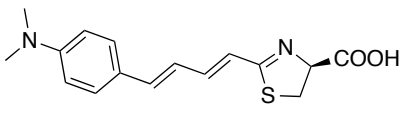

AkaLumine (**1a**)

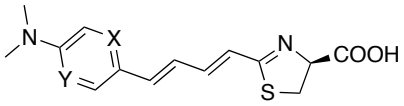

1b; X = CH, Y = N
1c; X = N, Y = CH
1d; X = N, Y = N

Scheme 1. Structures of firefly luciferin (LH_2), AkaLumine (**1a**), and the *N*-aryl analogues **1b–d**.

2.2. Synthesis of *N*-aryl analogues 1b–d

2.2.1. 5-cyano-2-dimethyl amino pyridine (3b). To a solution of 2-amino-5-cyianopyridine (**2b**) (1190 mg, 10.0 mmol) in tetrahydrofuran (100 mL), iodomethane (2.83 mL, 45.5 mmol) was added and the mixture was stirred at 0 °C. The mixture was slowly added sodium hydride (60% in oil, 1440 mg, 36.0 mmol) and stirred for 12 h. The reaction mixture was added methanol (20 mL) to quench the reaction. Further, the reaction mixture was added water and extracted with ethyl acetate (3 × 200 mL). The combined organic layers were dried over Na_2SO_4, filtered, and the solvents were concentrated under reduced pressure. The obtained residue was purified by silica gel column chromatography (hexane/ethyl acetate = 1/1) to yield dimethyl amino **3b** (1120 mg, 7.62 mmol, 76%) as a dark brown solid: mp 64; IR (neat, ν, cm^{-1}): 2213, 1324, 809; ^{1}H-NMR (500 MHz, $CDCl_3$) δ 8.41 (d, J = 2.3 Hz, 1H), 7.59 (dd, J = 9.2, 2.3 Hz, 1H), 6.48 (d, J = 9.2 Hz, 1H), 3.16 (s, 6H); ^{13}C-NMR (126 MHz, $CDCl_3$) δ 159.7, 152.7, 139.3, 119.1, 105.1, 95.3, 38.0; HR-ESI-MS: *m/z*: $[M+H]^+$ calculated for $C_{12}H_{10}N_3$, 148.0875; found, 148.0873.

Dimethyl amino **3c** and **3d** were prepared with a similar procedure to the preparation of **3b**. **2-cyiano-5-dimethyl amino pyridine** (**3c**) (yield 80%), dark brown solid: mp 65; IR (neat, ν, cm^{-1}): 2215, 1368, 822; ^{1}H-NMR (500 MHz, $CDCl_3$) δ 8.11 (d, J = 3.4 Hz, 1H), 7.47 (d, J = 9.2 Hz, 1H), 6.88 (dd, J = 8.9, 3.2 Hz, 1H), 3.09 (s, 6H); ^{13}C-NMR (126 MHz, $CDCl_3$) δ 147.1, 135.4, 129.0, 119.0, 118.9, 116.4, 39.7; HR-ESI-MS: *m/z*: $[M+H]^+$ calculated for $C_8H_{10}N_3$, 148.0875; found, 148.0880. **5-bromo-2-dimethyl amino pyrazine** (**3d**) (yield 80%), light yellow solid: mp 69; IR (neat, ν, cm^{-1}): 2852, 1378, 998; ^{1}H-NMR (500 MHz, $CDCl_3$) δ 8.11 (s, 1H), 7.75 (s, 1H), 3.10 (s, 6H); ^{13}C-NMR (126 MHz, $CDCl_3$) δ 153.9, 143.7, 129.1, 124.6, 37.8; HR-ESI-MS: *m/z*: $[M+H]^+$ calculated for $C_6H_9N_3Br_1$, 201.9980; found, 201.9990.

2.2.2. 5-aldehyde-2-dimethyl amino pyridine (4b). To a solution of dimethyl amino **3b** (1120 mg, 7.63 mmol) in dry toluene (20 mL) under Ar at 0 °C was slowly added, 1.0 M diisobutylaluminium hydride (DIBAL-H) in toluene (12 mL). After stirred for 30 min at 0 °C, the mixture was allowed to warm to r.t. and stirred 1 h. Then the reaction mixture was added acetone (10 mL) to decompose the excess reducing agent. Further, the mixed solution was added aqueous sodium potassium tartrate (50 mL), ethyl acetate (10 mL) and stirred overnight. The mixed solution was extracted with ethyl acetate (3 x 100 mL). The combined organic layers were dried over Na_2SO_4, filtered, the solvents were concentrated under reduced pressure. The obtained residue was purified by silica gel column chromatography (hexane/ethyl acetate = 1/1 to 0/1) to yield arylaldehyde **4b** (700 mg, 4.67 mmol, 61%) as a light-yellow solid: mp 54; IR (neat, ν, cm^{-1}): 2709, 1679, 1386, 815; ^{1}H-NMR (500 MHz, $CDCl_3$) δ 9.77 (s, 1H), 8.56 (d, J = 2.3 Hz, 1H), 7.92 (dd, J = 9.2, 2.3 Hz, 1H), 6.56 (d, J = 8.6 Hz, 1H), 3.21 (s, 6H); ^{13}C-NMR (126 MHz, $CDCl_3$) δ 189.2, 161.4, 154.6, 136.0, 121.7, 105.7, 38.2; HR-ESI-MS: *m/z*: $[M+H]^+$ calculated for $C_8H_{11}N_2O_1$, 151.0871; found, 151.0873.

Arylaldehyde **4c** were prepared with a similar procedure to the preparation of **4b**. **2-aldehyde-5-dimethyl amino pyridine** (**4c**) (yield 50%), light yellow solid: mp 69; IR (neat, ν, cm^{-1}): 2787, 1656, 1364, 825; ^{1}H-NMR (500 MHz, $CDCl_3$) δ 9.86 (s, 1H), 8.15 (s, 1H), 7.80 (d, J = 8.6 Hz, 1H), 6.92 (d, J = 9.2 Hz, 1H), 3.10 (s, 6H); ^{13}C-NMR (126 MHz, $CDCl_3$) δ 191.3, 147.9, 141.2, 133.6, 123.1, 116.2, 39.4; HR-ESI-MS: *m/z*: $[M+H]^+$ calculated for $C_8H_{11}N_2O_1$, 151.0871; found, 151.0848.

2.2.3. 5-aldehyde-2-dimethyl amino pyridine (4d). To a solution of dimethyl amino **3d** (1370 mg, 6.82 mmol) in dry tetrahydrofuran (50 mL) under Ar at -80 °C was slowly added 1.57 M *n*-butyllithium hydride (*n*-BuLi) in hexane (10.8 mL). After stirred for 60 min at -80 °C, the mixture was added *N*,*N*-dimethylformamide (DMF) (2.0 mL, 26 mmoL) and allowed to warm to r.t. After stirred for 1 h, the reaction mixture was added water to decompose the excess reducing agent. Further, the mixed solution was added water and extracted with ethyl acetate (3 x 200 mL). The combined organic layers were dried over Na_2SO_4, filtered, and the solvents were concentrated under reduced pressure. The residue obtained was purified by silica gel column chromatography (hexane/ethyl acetate = 1/1) to yield arylaldehyde **4d** (975 mg, 6.46 mmol, 95%) as a light yellow solid: mp 112; IR (neat, ν, cm^{-1}): 2783, 1681, 1373, 1008; ^{1}H-NMR (500 MHz, $CDCl_3$) δ 9.91 (s, 1H), 8.69 (s, 1H), 8.08 (d, J = 1.1 Hz, 1H), 3.26 (s, 6H); ^{13}C-NMR (126 MHz, $CDCl_3$) δ 190.7, 155.5, 144.3, 136.8, 129.4, 37.9; HR-ESI-MS: *m/z*: $[M+H]^+$ calculated for $C_7H_{10}N_3O_1$, 152.0824; found, 152.0814.

2.2.4. Ethyl (2*E*,4*E*)-5-(6-(dimethylamino)pyridin-3-yl)penta-2,4-dienoate (5b). Sodium hydride (60% in oil, 342 mg, 14.3 mmol) was slowly added to a solution of 5-aldehyde-2-dimethylaminopyridine (**4b**) (600 mg, 4.00 mmol) and triethyl 4-phosphonocrotonate (1.5 mL, 12 mmol) in dry tetrahydrofuran (50 mL) at 0 °C, and the mixture was stirred for 30 min. Ethanol (10 mL) was added to the reaction mixture for quenching and the product was extracted with ethyl acetate (3 × 50 mL). The combined organic layer was dried over Na_2SO_4, concentrated under reduced pressure. The residue was purified by silica gel column chromatography (hexane/ethyl acetate = 2/1) to yield ethyl 2,4-pentadienoate **5b** (433 mg, 1.76 mmol, 44%) as a light-yellow solid: mp 95; IR (neat, ν, cm^{-1}): 2903, 1704, 1386, 988, 805; ^{1}H-NMR (500 MHz, $CDCl_3$) δ 8.19 (d, J = 2.3 Hz, 1 H), 7.62 (dd, J = 9.2, 2.3 Hz, 1 H), 7.43 (dd, J = 15.2, 11.2 Hz, 1 H), 6.79 (d, J = 15.5 Hz, 1 H), 6.66 (dd, J = 15.5, 10.9 Hz, 1 H), 6.51 (d, J = 8.6 Hz, 1 H), 5.89 (d, J = 15.5 Hz, 1 H), 4.22 (q, J = 7.1 Hz, 2 H), 3.13 (s, 6 H), 1.31 (t, J = 6.9 Hz, 3 H); ^{13}C-NMR (126 MHz, $CDCl_3$) δ 167.3, 145.5, 144.8, 142.2, 139.7, 134.9, 125.3, 123.7, 120.6, 117.9, 60.2, 39.9, 14.3; HR-ESI-MS: *m/z*: $[M+H]^+$ calculated for $C_{14}H_{19}N_2O_2$, 247.1447; found, 247.1447.

Ethyl 2,4-pentadienoate **5c** and **5d** were prepared with a similar procedure to the preparation of **5b**. **Ethyl (2*E*, 4*E*)-5-(5-(dimethylamino)pyridin-2-yl)penta-2,4-dienoate** (**5c**) (yield 74%), light yellow solid: mp 105; IR (neat, ν, cm^{-1}): 2898, 1699, 1366, 1004, 815; ^{1}H-NMR (500 MHz, $CDCl_3$) δ 8.14 (d, J = 2.9 Hz, 1 H), 7.47 (dd, J = 15.5, 11.5 Hz, 1 H), 7.23 (d, J = 8.6 Hz, 1 H), 7.12 (dd, J = 15.2, 11.2 Hz, 1 H), 6.86–6.92 (m, 2 H), 5.99 (d, J = 14.9 Hz, 1 H), 4.22 (q, J = 7.1 Hz, 2 H), 3.03 (s, 6 H), 1.31 (t, J = 7.2 Hz, 3 H); ^{13}C-NMR (126 MHz, $CDCl_3$) δ 167.3, 145.5, 144.8, 142.2, 139.7, 134.9, 125.3, 123.7, 120.6, 117.9, 60.2, 39.9, 14.3; HR-ESI-MS: *m/z*: $[M+H]^+$ calculated for $C_{14}H_{19}N_2O_2$, 247.1447; found, 247.1454.

Ethyl (2*E*, 4*E*)-5-(5-(dimethylamino)pyrazin-2-yl)penta-2,4-dienoate (**5d**) (yield 65%), light yellow solid: mp 115–118; IR (neat, ν, cm^{-1}): 2942, 1699, 1398, 1006, 876; ^{1}H-NMR (500 MHz, $CDCl_3$) δ 8.05 (m, 2H), 7.46 (dd, J = 15.2, 11.7 Hz, 1 H), 7.14 (dd, J = 14.9, 11.5 Hz, 1 H), 6.84 (d, J = 15.5 Hz, 1 H), 5.99 (d, J = 15.5 Hz, 1 H), 4.22 (q, J = 7.1 Hz, 2 H), 3.17 (s, 6 H), 1.31 (t, J = 7.2 Hz, 3 H); ^{13}C-NMR (126 MHz, $CDCl_3$) δ 167.3, 153.8, 144.5, 142.3, 136.2, 129.9, 125.6, 121.1, 120.6, 60.3, 37.8, 14.4; HR-ESI-MS: *m/z*: $[M+Na]^+$ calculated for $C_{13}H_{17}N_3Na_1O_2$, 270.1219; found, 270.1213.

2.2.5. (2*E*, 4*E*)-5-(6-(dimethylamino)pyridin-3-yl)penta-2,4-dienoic acid (6b). To a solution of ethyl 2,4-pentadienoate **5b** (340 mg, 1.38 mmol) in 2-propanol (50 mL) was added 5 M NaOH aq. (560 μL), and the mixture was heated at reflux for 5 h. After cooling, the reaction mixture was neutralized by adding 4 M HCl aq. and concentrated under reduced pressure. The residue was purified by silica gel column chromatography (chloroform/methanol = 5/1) to give 2,4-pentadienoic acid **6b** （240 mg, 1.10 mmol, 80%） as a light yellow solid: mp 215–218; IR (neat, ν, cm^{-1}): 1674, 995, 802; ^{1}H-NMR (500 MHz, CD_3OD) δ 8.11 (d, J = 2.3 Hz, 1 H), 7.80 (dd, J = 9.2, 2.3 Hz, 1 H), 7.42 (dd, J = 15.2, 10.0 Hz, 1 H), 6.80–6.89 (m, 2 H), 6.70 (d, J = 9.2 Hz, 1 H), 5.90 (d, J = 14.9 Hz, 1 H), 3.12 (s, 6 H); ^{13}C-NMR (126 MHz, CD_3OD) δ 171.2, 160.1, 149.1, 147.1, 138.8, 135.9, 124.0, 121.7, 120.4, 107.8, 38.5; HR-ESI-MS: *m/z*: $[M+H]^+$ calculated for $C_{12}H_{15}N_2O_2$, 219.1134; found, 219.1122.

2,4-pentadienoic acid **6c** and **6d** were prepared with a similar procedure to the preparation of **6b**. **(2*E*, 4*E*)-5-(5-(dimethylamino)pyridin-2-yl)penta-2,4-dienoic acid** (**6c**) (crude 115%), light green solid: mp 230; IR (neat, ν, cm^{-1}): 3428, 1709, 986, 807; ^{1}H-NMR (500 MHz, DMSO-D6) δ 8.12 (d, J = 2.9 Hz, 1 H), 7.50 (br, 1 H), 7.35 (dd, J = 14.9, 11.5 Hz, 1 H), 7.17–7.22 (m, 2 H), 6.99 (d, J = 14.9 Hz, 1 H), 6.00 (d, J = 15.5 Hz, 1 H), 3.01 (s, 6 H); ^{13}C-NMR (126 MHz, CD_3OD) δ 147.4, 143.4, 139.2, 134.6, 127.5, 124.4, 120.4, 40.0; HR-ESI-MS *m/z*: $[M+H]^+$ calculated for $C_{12}H_{15}N_2O_2$, 219.1134; found, 219.1128. **(2E, 4E)-5-(5-(dimethylamino)pyrazin-2-yl)penta-2, 4-dienoic acid** (**6d**) (yield 84%), light yellow solid: mp 232; IR (neat, ν, cm^{-1}): 1674, 1261, 995; ^{1}H-NMR (500 MHz, CD_3OD) δ 8.11 (s, 1 H), 8.07 (s, 1 H), 7.28 (dd, J = 15.2, 11.2 Hz, 1 H), 7.12 (dd, J = 15.2, 11.2 Hz, 1 H), 6.81 (d, J = 15.5 Hz, 1 H), 6.01 (t, J = 15.2 Hz, 1 H), 3.16 (s, 6 H); ^{13}C-NMR (126 MHz, CD_3OD) δ 174.1, 155.2, 142.9, 138.7, 135.1, 131.0, 127.9, 38.0, 30.8; HR-ESI-MS: *m/z*: $[M+H]^+$ calculated for $C_{11}H_{13}N_3Na_1O_2$, 242.0906; found, 242.0908.

2.2.6. Methyl *N*-((2*E*,4*E*)-5-(6-(dimethylamino)pyridin-3-yl)penta-2,4-dienoyl)-*S*-trityl-*D*-cysteinate (7b). To a solution of 2,4-pentadienoic acid **6b** (126 mg, 0.578 mmol) and *S*-trityl-*D*-cysteine methyl ester (261 mg, 0.692 mmol) in DMF (50 mL), was added 1-(3-dimethylaminopropyl)-3-ethylcarbodiimide hydrochloride (EDC·HCl) (278 mg, 1.45 mmol) and *N*,*N*-dimethyl-4-aminopyridine (DMAP) (141 mg, 1.15 mmol), and the reaction mixture was stirred for 2 h at r.t. The reaction was quenched by adding water (50 mL) and the product was extracted with ethyl acetate (3 × 50 mL). The combined organic layer was dried over Na_2SO_4, filtered, and concentrated under reduced pressure. The residue was purified by silica gel column chromatography (hexane/ethyl acetate =1/1) to yield amide **7b** (264 mg, 0.457 mmol, 79%) as a light yellow solid: mp 85; IR (neat, ν, cm^{-1}): 1738, 1651, 1586, 741, 697; ^{1}H-NMR (500 MHz, $CDCl_3$) δ 8.20 (d, J = 2.3 Hz, 1 H), 7.62 (dd, J = 9.2, 2.3 Hz, 1 H), 7.20–7.39 (m, 17 H), 6.77 (d, J = 15.5 Hz, 1 H), 6.65 (dd, J = 15.2, 11.2 Hz, 1 H), 6.51 (d, J = 9.2 Hz, 1 H), 5.95 (d, J = 8.0 Hz, 1 H), 5.84 (d, J = 14.9 Hz, 1 H), 4.74 (dd, J = 12.6, 5.2 Hz, 1 H), 3.72 (s, 3 H), 3.13 (s, 6 H), 2.70 (t, J = 4.6 Hz, 2 H); ^{13}C-NMR (126 MHz, $CDCl_3$) δ 171.1, 165.9, 158.8, 148.4, 144.3, 142.3, 137.0, 134.2, 129.4, 127.9, 126.79, 122.4, 121.0, 120.1, 105.8, 66.8, 52.5, 51.3, 38.0, 33.9; HR-ESI-MS: *m/z*: $[M+H]^+$ calculated for $C_{35}H_{36}N_3O_3S_1$, 578.2477; found, 578.2491.

Amide **7c** and **7d** were prepared with a similar procedure to the preparation of **7b**. **Methyl *N*-((2*E*,4*E*)-5-(5-(dimethylamino)pyridin-2-yl)penta-2,4-dienoyl)-*S*-trityl-*D*-cysteinate** (**7c**) (yield 79%), light yellow solid: mp 86; IR (neat, ν, cm^{-1}): 1738, 1651, 1575, 741, 697; ^{1}H-NMR (500 MHz, $CDCl_3$) δ 8.15 (d, J = 2.9 Hz, 1 H), 7.21–7.39 (m, 16 H), 7.13 (dd, J = 14.9, 11.5 Hz, 1 H), 6.92 (dd, J = 8.9, 3.2 Hz, 1 H), 6.85 (d, J = 15.5 Hz, 1 H), 5.90–5.94 (m, 2 H), 4.74 (dd, J = 12.9, 5.4 Hz, 1 H), 3.73 (s, 3 H), 3.03 (s, 6 H), 2.74 (q, J = 6.1 Hz, 1 H), 2.68 (dd, J = 12.3, 4.9 Hz, 1 H); ^{13}C-NMR (126 MHz, $CDCl_3$) δ 171.0, 165.6, 145.4, 144.3, 142.5, 142.1, 139.0, 134.9, 129.5, 128.0, 126.9, 125.4, 123.7, 122.5, 118.0, 67.0, 52.7, 51.1, 40.0, 34.0; HR-ESI-MS: *m/z*: $[M+H]^+$ calculated for $C_{35}H_{36}N_3O_3S_1$, 578.2477; found, 578.2478. **Methyl *N*-((2*E*,4*E*)-5-(5-(dimethylamino)pyrazin-2-yl)penta-2,4-dienoyl)-*S*-trityl-*D*-cysteinate** (**7d**) (yield 84%), light yellow solid: mp 70; IR (neat, ν, cm^{-1}): 1738, 1651, 1569, 741, 697; ^{1}H-NMR (500 MHz, $CDCl_3$) δ 8.05 (s, 2 H), 7.20–7.44 (m, 15 H), 7.13 (dd, J = 14.9, 11.5 Hz, 1 H), 6.82 (d, J = 14.9 Hz, 1 H), 5.93 (m, 2 H), 4.74 (d, J = 8.0 Hz, 1 H), 3.73 (s, 3 H), 3.18 (s, 6 H), 2.67–2.73 (m, 2 H); ^{13}C-NMR (126 MHz, $CDCl_3$) δ 171.0, 165.6, 153.8, 144.3, 142.2, 141.8, 137.3, 135.6, 129.8, 129.6, 129.5, 128.0, 128.0, 126.9, 126.8, 125.6, 122.9, 67.0, 52.7, 51.2, 37.8, 34.0; HR-ESI-MS: *m/z*: $[M+H]^+$ calculated for $C_{34}H_{34}N_4Na_1O_3S_1$, 601.2249; found, 601.2243.

2.2.7. Methyl (*S*)-2-((1*E*,3*E*)-4-(6-(dimethylamino)pyridin-3-yl)buta-1,3-dien-1-yl)-4,5-dihydrothiazole-4-carboxylate (8b). To a solution of amide **7b** (191 mg, 0.331 mmol) in dichloromethane (10 mL) was added trifluoromethanesulfonic anhydride (Tf_2O) (170 μL, 1.00 mmol) under Ar at 0 °C and the mixture was stirred for 10 min. Ion exchange resin IRA400 OH AG was added to the reaction mixture for neutralization. The resin was filtered through a cotton plug and washed thoroughly with methanol. The filtrate was concentrated *in vacuo*. The crude products were purified by PTLC (hexane/ethyl acetate = 2/1) to yield thiazolidine ester **8b** (51.6 mg, 0.163 mmol, 48%) as yellow solid: mp 134; IR (neat, ν, cm^{-1}): 2914, 1746, 1588, 1201,994, 799; ^{1} H-NMR (500 MHz, $CDCl_3$) δ 8.17 (d, J = 2.3 Hz, 1 H), 7.64 (dd, J = 9.2, 2.3 Hz, 1 H), 6.93 (dd, J = 15.5, 9.7 Hz, 1 H), 6.68–6.75 (m, 2 H), 6.50–6.56 (m, 2 H), 5.17 (t, J = 8.9 Hz, 1 H), 3.83 (s, 3 H), 3.59 (dd, J = 11.5, 9.2 Hz, 1 H), 3.53 (dd, J = 10.9, 9.2 Hz, 1 H), 3.13 (s, 6 H); ^{13}C-NMR (126 MHz, $CDCl_3$) δ 171.4, 170.2, 159.0, 148.8, 143.3, 136.3, 134.1, 123.3, 123.1, 120.2, 105.9, 77.9, 52.8, 38.1, 34.6; HR-ESI-MS: *m/z*: $[M+H]^+$ calculated for $C_{16}H_{20}N_3O_2S_1$, 318.1276; found, 318.1271.

Thiazolidine-ester **8c** and **8d** were prepared with a similar procedure to the preparation of **8b**. **Methyl (*S*)-2-((1*E*,3*E*)-4-(5-(dimethylamino)pyridin-2-yl)buta-1,3-dien-1-yl)-4,5-dihydrothiazole-4-carboxylate** (**8c**) (yield 63%), brown solid: mp 117; IR (neat, ν, cm^{-1}): 2949, 1725, 1576, 1206, 987; ^{1}H-NMR (500 MHz, $CDCl_3$) δ 8.14 (d, J = 3.4 Hz, 1 H), 7.22 (d, J = 8.6 Hz, 1 H), 7.15 (dd, J = 14.9, 10.9 Hz, 1 H), 6.90–6.99 (m, 2 H), 6.81 (d, J = 15.5 Hz, 1 H), 6.65 (d, J = 15.5 Hz, 1 H), 5.17 (t, J = 9.2 Hz, 1 H), 3.83 (s, 3 H), 3.61 (t, J = 10.0 Hz, 1 H), 3.54 (t, J = 10.0 Hz, 1 H), 3.03 (s, 6 H); ^{13}C-NMR (126 MHz, $CDCl_3$) δ 171.4, 170.1, 145.4, 142.8, 142.5, 138.0, 134.9, 126.2, 125.0, 123.6, 118.0, 77.9, 52.8, 40.0, 34.5; HR-ESI-MS: *m/z*: $[M+H]^+$ calculated for $C_{16}H_{20}N_3O_2S_1$, 318.1276; found, 318.1271. **Methyl (*S*)-2-((1*E*,3*E*)-4-(5-(dimethylamino)pyrazin-2-yl)buta-1,3-dien-1-yl)-4,5-dihydrothiazole-4-carboxylate** (**8d**) (yield 44%)

yellow solid: mp 142; IR (neat, ν, cm^{-1}): 2940, 1745, 1574, 1197, 982; ^{1}H-NMR (500 MHz, $CDCl_3$) δ 8.04 (s, 2 H), 7.14–7.20 (m, 1 H), 6.94–6.99 (m, 1 H), 6.77 (d, J = 14.9 Hz, 1 H), 6.65 (d, J = 15.5 Hz, 1 H), 5.17 (t, J = 8.9 Hz, 1 H), 3.83 (s, 3 H), 3.54–3.63 (m, 2 H), 3.17 (s, 6 H); ^{13}C-NMR (126 MHz, $CDCl_3$) δ 171.3, 170.0, 153.7, 142.5, 142.2, 137.3, 134.5, 129.9, 126.4, 125.3, 78.0, 52.8, 37.8, 34.6; HR-ESI-MS: *m/z*: $[M+H]^+$ calculated for $C_{15}H_{19}N_4O_2S_1$, 319.1229; found, 319.1230.

2.2.8.
(*S*)-2-((1*E*,3*E*)-4-(6-(dimethylamino)pyridin-3-yl)buta-1,3-dien-1-yl)-4,5-dihydrothiazole-4-carboxylic acid (1b). A solution of thiazolidine ester **8b** (147 mg, 0.463 mmol) in 6 M HCl aq. (30 mL) was stirred at r.t. for 18 h. After the reaction mixture was added sodium bicarbonate to neutralize, the mixture was concentrated under reduced pressure. The crude products were purified by automated flash chromatography system (Smart Flash EPCLC AI-580S, ULTRAPACK COLUMNS C_{18}, H_2O/ methanol = 9/1 to 1/9) to yield *N*-aryl luciferin analogue **1b** (101 mg, 0.332 mmol, 72 %) as an orange solid: mp 258–261; IR (neat, ν, cm^{-1}): 3360, 1589, 983; ^{1}H-NMR (500 MHz, DMSO-D6) δ 8.17 (d, J = 2.3 Hz, 1 H), 7.78 (dd, J = 8.6, 2.3 Hz, 1 H), 6.74–6.92 (m, 3 H), 6.67 (d, J = 9.2 Hz, 1 H), 6.52 (d, J = 14.9 Hz, 1 H), 4.71 (t, J = 8.9 Hz, 1 H), 3.49 (dd, J = 10.3, 9.2 Hz, 1 H), 3.30–3.41 (m, 1 H), 3.06 (s, 6 H); ^{13}C-NMR (126 MHz, DMSO-D6) δ 172.0, 163.1, 158.6, 148.1, 140.7, 134.8, 134.2, 124.5, 123.5, 120.2, 106.0, 83.2, 37.7, 35.4; HR-ESI-MS: *m/z*: $[M+H]^+$ calculated for $C_{15}H_{18}N_3O_2S_1$, 304.1120; found, 304.1100; 90%*e.e.* from chiral HPLC (retention time of L-isomer: 8.60 min, D-isomer: 20.2 min, Formic acid buffer at pH 2.0/methanol = 10/90, detection of UV: 360 nm).
N-aryl luciferin analogue **1c** and **1d** were prepared with a similar procedure to the preparation of **1b**.
(*S*)-2-((1*E*,3*E*)-4-(5-(dimethylamino)pyridin-2-yl)buta-1,3-dien-1-yl)-4,5-dihydrothiazole-4-carboxylic acid (**1c**) (yield 63%) yellow solid: mp 207; IR (neat, ν, cm^{-1}): 3207, 1575, 984; ^{1}H-NMR (500 MHz, DMSO-D6) δ 8.12 (d, J = 3.4 Hz, 1 H), 7.33 (d, J = 8.6 Hz, 1 H), 7.15 (dd, J = 15.5, 10.9 Hz, 1 H), 7.05 (dd, J = 8.6, 2.9 Hz, 1 H), 6.80–6.88 (m, 2 H), 6.62 (d, J = 14.9 Hz, 1 H), 4.76 (t, J = 8.9 Hz, 1 H), 3.50 (t, J = 9.5 Hz, 1 H), 3.33–3.37 (m, 1 H), 2.98 (s, 6 H); ^{13}C-NMR (126 MHz, DMSO-D6) δ 171.7, 163.3, 145.3, 142.1, 140.2, 137.0, 134.7, 126.0, 125.9, 123.2, 118.1, 82.9, 39.2, 35.4; HR-ESI-MS: *m/z*: $[M+H]^+$ calculated for $C_{15}H_{18}N_3O_2S_1$, 304.1120; found, 304.1107; 90%*e.e.* from chiral HPLC (retention time of L-isomer: 12.1 min, D-isomer: 15.5 min, Formic acid buffer at pH 2.0/methanol = 10/90, detection of UV: 400 nm).
(*S*)-2-((1*E*,3*E*)-4-(5-(dimethylamino)pyrazin-2-yl)buta-1,3-dien-1-yl)-4,5-dihydrothiazole-4-carboxylic acid (**1d**) (yield 37%) yellow solid: mp 204–207; IR (neat, ν, cm^{-1}): 3234, 1568, 1386, 982; ^{1}H-NMR (500 MHz, CD_3OD) δ 8.13 (s, 1 H), 8.09 (s, 1 H), 7.18 (dd, J = 15.2, 11.2 Hz, 1 H), 7.04 (dd, J = 15.5, 10.9 Hz, 1 H), 6.86 (d, J = 15.5 Hz, 1 H), 6.61 (d, J = 14.9 Hz, 1 H), 5.06 (t, J = 8.9 Hz, 1 H), 3.59 (m, 2 H), 3.17 (s, 6 H); ^{13}C-NMR (126 MHz, CD_3OD) δ 176.2, 171.9, 155.4, 144.1, 143.4, 138.5, 136.2, 131.3, 127.7, 125.7, 80.3, 38.1, 36.4; HR-ESI-MS: *m/z*: $[M+H]^+$ calculated for $C_{14}H_{17}N_4O_2S_1$, 305.1072; found, 305.1077; 87%*e.e.* from chiral HPLC (retention time of L-isomer: 19.6 min, D-isomer: 26.5 min, 0.1 M Potassium hexafluorophosphate buffer at pH 2.0/ acetonitrile = 65/35, detection of UV: 450 nm).

2.3. Measurement of solubility in PBS. The solubility of each compound in PBS (1×, pH 7.4, gibco® by lifetechnologies™) at 25 °C was determined by UV/vis absorption measurement. Molar extinction coefficients (ε) of **1a–d** in PBS were initially determined (Table 1 and Figure S1). Then, a saturated solution of each compound was prepared at 25 °C and absorbance of an appropriately diluted solution of the saturated one was measured to give the maximum concentration (c_{max}).

2.4. Luminescence measurements
2.4.1. Measurement of bioluminescence activity. The bioluminescence activities of **1b–d** together with those of LH_2 and **1a**[16] were investigated using *Ppy* luciferase. The substrates were dissolved in 50 mM KPB (pH 6.0), *Ppy* luciferase was dissolved in 50 mM KPB (pH 8.0) containing 10% glycerol, and Mg-ATP was dissolved in ultrapure water. An L-L reaction was initiated by injection of 10 μL of Mg-ATP (200 μM) into a mixture of 5 μL of a substrate solution (100 μM), 5 μL of luciferase solution (1 mg/mL), and 5 μL of KPB (500 mM, pH 8.0). Light emission was monitored in the range 400–750 nm in increments of 1 nm for 180 s to provide emission spectra. Light intensity was determined as the intensity of the emission spectrum at the λ_{BL} value.

2.4.2. Measurement of K_m and V_{max} values. For Lineweaver-Burk analysis, the light emission from an L-L reaction was monitored with the ATTO AB-2270 luminometer for 30 s with sampling intervals of 0.1 s. Emission intensities were expressed as counts per second (cps). The L-L reaction was initiated by injecting 40 μL of Mg-ATP (200 μM) into a mixture of 20 μL of a substrate solution (100 μM) 20 μL luciferase solution (0.1 mg/mL), and 20 μL KPB (500 mM, pH 8.0) at room temperature. The substrates were dissolved in 50 mM KPB (pH 6.0), *Ppy* luciferase (1mg/mL in 50 mM KPB containing 10% glycerol, pH 8.0) was dissolved to 0.1 mg/mL by 50 mM KPB (pH 6.0) containing 35% glycerol, and Mg-ATP was dissolved in ultrapure water. The final concentrations of the substrates were varied from 0.02 to 100 μM. The K_m and V_{max} values of the substrates were determined from the integrated values of emission intensities and calculated using Lineweaver-Burk plots with the Enzyme Kinetics Wizard module in the commercially available SigmaPlot 13.0 software package (Systat Software Inc.).

2.4.3. Measurement of chemiluminescence activity. Analogues **1b–d** were treated with propylphosphonic anhydride (T_3P) and triethylamine (NEt_3) according to a previously published protocol.[28] A chemiluminescence reaction was initiated by injecting 150 μL T_3P (150 mM) in DMF into a mixture of 40 μL of a substrate (20 mM) in DMF and 40 μL NEt_3 (500 mM) in DMF. Chemiluminescence spectra of the substrates were measured with the ATTO AB-1850 spectrophotometer in the range 400–750 nm in increments of 1 nm for 180 s.

2.5. Cell and animal imaging
2.5.1. Cell culture. The murine Lewis lung carcinoma cell line LLC was obtained from ATCC (Rockville, MD, USA). LLC/luc was established with a luc+ gene as previously described.[20] LLC/mKO_2-Rluc8.6 were established as previously described.[20,29] The cells were maintained at 37 °C in Dulbecco's modified essential medium (Nacalai Tesque) supplemented with 5% fetal calf serum, penicillin (100 units/mL), and streptomycin (100 μg/mL) and regularly checked for mycoplasma contamination using a mycoplasma check kit (Lonza).

2.5.2. Cellular imaging. The substrates were reacted with LLC/luc (2×10^5 cells/well) in a black 96-well plate.

Bioluminescence was measured using IVIS Spectrum 1 min after adding the substrates. The following conditions were used for image acquisition: open (for total bioluminescence) or 680 ± 10 nm using an emission filter (for NIR bioluminescence), exposure time = 10 s, binning = medium: 8, field of view = 12.9 × 12.9 cm, and f/stop = 1. The bioluminescence images were analyzed using Living Image 4.3 software (PerkinElmer) specialized for IVIS.

2.5.3. Cell viability assay. LLC/mKO$_2$-Rluc8.6 cells (2×10^4 cells/well) were seeded into a 24-well plate. After 24-h incubation, the cells were further cultured for 24-h with the substrate at the indicated concentration. Then, the cells in each well were harvested to prepare cell lysates and their Rluc bioluminescence activity was measured using a GL-201A luminometer.

2.5.4. Mice. C57B/6 albino mice (female and male, six weeks old) were obtained from Charles River Laboratory Japan (Yokohama, Japan). All the experimental procedures using mice have been previously approved by the Animal Experiment Committees of the Tokyo Institute of Technology (authorization number 2014005) and carried out in accordance with the relevant national and international guidelines.

2.5.5. Tumor models. For subcutaneous tumor models, LLC/luc (3×10^5 cells/10 μL) suspended in PBS was mixed with an equal volume of Geltrex® (Invitrogen, Thermo Fisher Scientific) and subcutaneously injected into C57B/6 albino mice (female). The experiments were performed 4 days after injection. For the lung metastasis model, LLC/luc (5×10^5 cells/100 μL) suspended in PBS was injected into the tail vein of C57B/6 albino mice (male). The experiments were performed 10–20 days after intravenous injection.

2.5.6. Animal imaging. Bioluminescence images of subcutaneous tumors and lung metastasis were sequentially acquired with IVIS Spectrum every 3 min for 30 min after intraperitoneal injection with 100 μL of 33 mM substrates, and the highest bioluminescence intensities among the acquired images were selected for analysis. For comparing bioluminescence production between different substrates using the same mice, the images for analogue **1c** were acquired 4-h after injection of LH$_2$, in which the effect of LH$_2$ had completely disappeared.[20] The following conditions were used for image acquisition: open emission filter, exposure time = 60 s, binning = medium: 8, field of view = 12.9 × 12.9 cm, and f/stop = 1. The bioluminescence images were analyzed using Living Image 4.3 software (PerkinElmer) specialized for IVIS.

2.5.7. Statistical analysis. Data are presented as means ± standard error of the mean and were statistically analyzed with a two-side Student's t-test. P values of less than 0.05 were considered statistically significant.

3. Results and Discussion

3.1. Synthesis of *N*-aryl analogues of AkaLumine. The analogues **1b**, **1c**, and **1d**, which have a pyridine or pyrazine ring in place of the benzene ring of **1a** (Scheme 1), were designed to have superior aqueous solubilities to that of **1a** while maintaining its bioluminescence activity. The *N*-aryl analogues **1b–d** were synthesized by a procedure similar to that for **1a** (Scheme 2). As key synthetic intermediates, arylaldehydes **4b–d** were prepared from the corresponding commercially available aminonitriles and aminobromide. Arylaldehydes **4b** and **4c** were prepared by dimethylation of aminonitriles followed by DIBAL-H reduction. Arylaldehyde **4d** was prepared by dimethylation of 5-bromo-2-pyrazinecarbonitrile followed by formylation via the lithiated anion. Horner-Wadsworth-Emmons reactions of **4b–d** with triethyl 4-phosphonocrotonate afforded 5-aryl-2,4-pentadienoates **5b–d**, which were hydrolyzed to give carboxylic acids **6b–d**. Condensations of **6b–d** with *S*-trityl-*D*-cysteine methyl ester gave amides **7b–d**, and the following thiazole ring formations with Tf_2O afforded esters **8b–d**. Finally, acid hydrolysis of **8b–d** produced the target analogues **1b–d**.

3.2. Water solubilities of 1b–d. The maximum concentrations (c_{max}) of **1b**, **1c**, and **1d** in PBS at pH 7.4 and 25 °C were determined to be 28, 69, and 480 mM, respectively (Table 1). Thus, the c_{max} values of **1b–d** are greater than that of **1a** (2.2 mM) (Table 1), indicating substituting the benzene ring in the structure of **1a** with a pyridine or pyrazine ring is an effective means of improving water solubility. Clearly, the pyrazine analogue **1d** has the highest water solubility among the *N*-aryl analogues. Interestingly, the 2-pyridyl analogue **1c** exhibits superior water solubility to that of the 3-pyridyl analogue **1b**, despite **1b** and **1c** differing only in the position of the pyridyl nitrogen.

Table 1. Electronic absorption properties and water solubilities of **1a–d** in PBS (1×, pH 7.4) at 25 °C

Compound	λ_{max}/nm ($\varepsilon/10^5$ dm^3 mol^{-1} cm^{-1})[a]	c_{max}[b] /mM
1a	370 (2.2)	2.2
1b	375 (2.1)	28
1c	375 (1.6)	69
1d	390 (1.4)	480

[a]Absorption maximum of the lowest-energy absorption band (λ_{max}). Molar extinction coefficient (ε) given in parentheses.
[b]The maximum concentrations (c_{max}) in PBS (pH 7.4) at 25 °C.

3.3. Luminescence properties of 1b–d. Since the luciferase of the North American firefly *Photinus pyralis* (*Ppy*) is commonly used in the L-L reaction for BLI, we investigated the bioluminescence activity with *Ppy* luciferase. The L-L reactions with *Ppy* luciferase of **1b–d** together with those of LH$_2$ and **1a** in potassium phosphate buffer (KPB) at pH 8.0 in the presence of ATP and Mg^{2+} under air were investigated. The bioluminescence properties of **1a–d** and LH$_2$ are summarized in Table 2. **1b–d** show moderate luminescence activities. The light intensities (Rel. Int.) during the initial 180 s for **1a–d** are 36%, 135%, 10%, and 4%, respectively, as relative values compared with that of LH$_2$ (Table 2), indicating that **1b–d** have moderate luminescence activities. Emission maxima (λ_{BL}) in the bioluminescence spectra of **1b**, **1c**, and **1d** are observed at 640, 675, and 625 nm, respectively (Figure 1A and Table 2). Thus, the λ_{BL} values of all the new analogues are red-shifted compared to that of LH$_2$. The λ_{BL} values for **1b** and **1d** are blue-shifted by 35 and 50 nm, respectively, compared to that of **1a**, while **1c** exhibits a similar λ_{BL} value to that of **1a** (Figure 1A and Table 2). To investigate the cause of the variation in λ_{BL}

values for **1b–d**, chemiluminescence reactions of **1a–d** were performed in DMF containing T_3P and NEt_3 under air.[28] The chemiluminescence emission maxima (λ_{CL}) of **1a–d** are observed at 645, 600, 635, and 595 nm, respectively (Figure 1B and Table 2). Much like the variation in the λ_{BL} values of **1b–d**, **1b** and **1d** exhibit 45 and 50 nm blue-shifted λ_{CL} values, respectively, compared with that of **1a**, and the λ_{CL} value of **1c** is slightly blue-shifted (Figure 1B and Table 2). These results indicate that the λ_{BL} and λ_{CL} values of **1b–d** are largely determined by their π-electronic properties.

Table 2. Bio- and chemiluminescence properties of LH_2 and **1a–d**

Compound	Rel. Int[a]	λ_{BL}[b] /nm	λ_{CL}[c] /nm	K_m /μM	Rel. V_{max}[d]
LH_2	100%	560	620	107 ± 15[e]	–
1a	36%	675	645	1.3 ± 0.3	100%
1b	135%	640	600	29 ± 5	240%
1c	10%	675	635	6.2 ± 1.2	180%
1d	4%	625	595	57 ± 9	6.5%

[a]Relative light intensities at λ_{BL} for the L-L reactions of **1a–d** during the initial 180 s compared to that of LH_2.
[b]Bioluminesnce emission maximum.
[c]Chemiluminesnce emission maximum.
[d]Relative V_{max} during the initial 30 s for the L-L reactions of **1b–d** compared to that of **1a**. The concentration of Mg-ATP was 200 μM in H_2O.
[e]Ref.[20]

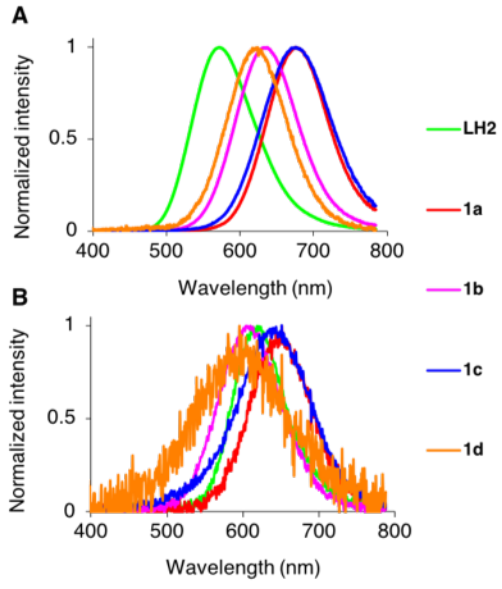

Figure 1. Emission spectra of bioluminescence (**A**) and chemiluminescence (**B**) of LH_2 and **1a–d**.

The kinetic constants (K_m and Rel. V_{max}) for **1a–d** were investigated by the previously reported method.[20] The K_m values of **1a–d** are 1.3, 29, 6.2, and 57 μM, respectively (Table 2). Thus, the K_m values of **1b–d** are greater than that of **1a**. This result corresponds with the observation that the water solubilities of **1b–d** are better than that of **1a**. In fact, the pyrazine-containing analogue **1d** has the largest K_m value among **1a–d**. Thus, the hydrophilicity of **1d** decreases its affinity with the luciferase active site. Interestingly, the K_m value of **1b** is approximately five-fold that of **1c**, indicating that the position of the N atom has a profound effect on affinity with the luciferase active site. The pyridine-containing analogues **1b** and **1c** exhibit greater Rel. V_{max} values than that of **1a**, and the pyrazine-containing analogue **1d** exhibits a smaller Rel. V_{max} value than that of **1a**. Because the Rel. V_{max} value reflects the bioluminescence quantum yield (Φ_{BL}) and rate constant of the enzymatic reaction (k_{cat}), the N atom in the *N*-aryl moieties affects interactions with the luciferase active site, thus largely determining the Φ_{BL} and k_{cat} values.

3.4. Density functional theory calculations for the light emitters generated from the bio- and chemiluminescence reactions of 1a–d. Oxyluciferin (OLH) is the light emitter in the L-L reaction of LH_2. While OLH in the ground state has the enol form as the most stable structure,[30,31] the excited state of OLH generated by the L-L reaction of LH_2 adopts the keto-phenolate form.[6,7,32] Thus, it is reasonable to assume that the keto forms of *oxy*-**1a–d** (Figure 2A) are the light emitters in the L-L reactions of **1a–d**.[18] To further investigate the observed λ_{BL} and λ_{CL} values for **1b–d**, the electronic properties of *oxy*-**1b–d** were investigated by density functional theory (DFT) and time-dependent DFT (TD-DFT) calculations with the B3LYP/6-31+G(d) method. The optimized structures of *oxy*-**1b–d** together with that of *oxy*-**1a**[18] are shown in Figure 2A and the calculation data are summarized in Table 3, which shows the energy levels of the HOMOs and LUMOs, the HOMO-LUMO energy gaps (ΔE_{H-L}), and the wavelengths (λ_{tr}), oscillator strengths (*f*), and configurations for the $S_0 \rightarrow S_1$ transitions in *oxy*-**1a–d**.

The electronic distributions for the HOMOs and LUMOs of *oxy*-**1b–d** are similar to those for *oxy*-**1a**. The HOMO and LUMO levels of *oxy*-**1b–d** are slightly lower than those of *oxy*-**1a** because *oxy*-**1b–d** contains an *N*-heterocycle instead of the benzene ring in *oxy*-**1a**. The ΔE_{H-L} values of *oxy*-**1b–d** are slightly higher than that of *oxy*-**1a**. The order of ΔE_{H-L} values (*oxy*-**1a** < *oxy*-**1c** < *oxy*-**1b** < *oxy*-**1d**) roughly corresponds to those of the λ_{BL} values (*oxy*-**1a** ≈ *oxy*-**1c** > *oxy*-**1b** > *oxy*-**1d**) and λ_{CL} values (*oxy*-**1a** > *oxy*-**1c** > *oxy*-**1b** > *oxy*-**1d**), indicating that the emission maximum wavelengths of bioluminescence and chemiluminescence for **1a–d** are mainly determined by the electronic properties of *oxy*-**1a–d**. Interestingly, however, the λ_{BL} values of **1a** and **1c** are similar, indicating that the emissions of the lowest excited singlet (S_1) states of *oxy*-**1a–d** generated by the L-L reactions are modulated by interactions with the luciferase active site.

Table 3. DFT and TD-DFT calculation data for *oxy*-**1a–d**

Compound	HOMO /eV	LUMO /eV	ΔE_{H-L}[a] /eV	λ_{tr}/nm (*f*)[b]	Configuration[c]

oxy-**1a**[d]	−5.54	−2.65	2.89	439 (1.38)	H → L (0.70)
oxy-**1b**	−5.76	−2.77	2.99	426 (1.43)	H → L (0.70)
oxy-**1c**	−5.70	−2.74	2.96	432 (1.29)	H → L (0.70)
oxy-**1d**	−5.91	−2.87	3.03	421 (1.37)	H → L (0.70)

[a]Energy difference between HOMO and LUMO.
[b]Wavelength estimated from the energy of the $S_0 \rightarrow S_1$ transition. Oscillator strengths (*f*) are in the parentheses.
[c]Configuration of excitation. Coefficients are in the parentheses. H and L denote HOMO and LUMO, respectively.
[d]Ref.[18]

The HOMOs of *oxy*-**1a–d** exhibit electronic distribution mainly at the (4-dimethylaminophenyl)-ethenyl moiety, and their LUMOs exhibit electronic distributions mainly at the 2-butadinenyl-1,3-thiazolone moiety (Figure 2B). Thus, electronic excitations in *oxy*-**1b–d** due to HOMO-LUMO transitions have charge-transfer characteristics, producing polarized excited singlet states. The electronic properties of the HOMOs and LUMOs of *oxy*-**1a–d** result in their large *f* values (over 1.2) for transitions from the ground (S_0) states to the lowest excited singlet (S_1) states (Table 3). Because the fluorescence emission process is the reverse process of the $S_0 \rightarrow S_1$ transition, a rate constant of fluorescence emission is predicted from the *f* value of the $S_0 \rightarrow S_1$ transition.[33] Thus, the *f* values for *oxy*-**1a–d** indicate that they are good light emitters.

3.5. Cellular imaging. For cellular and animal imaging experiments, we choose **1c** as a preferential *N*-aryl analogue, because the λ_{BL} value of **1c** is almost same as that of **1a**. In fact, it is known that a longer λ_{BL} value is more effective to improve a BL image in a deep animal tissue than a higher BL intensity.[20] At first, we investigated bioluminescence property of **1c** in culture cells together with that of **1a**. For the purpose, we treated murine Lewis lung carcinoma (LLC) constitutively expressing FLuc (LLC/luc) with various concentrations of LH_2, **1a**-HCl and **1c** (Figure 3A). Cells treated with **1c** emit robust NIR bioluminescence comparable with those treated with **1a**-HCl. Furthermore, **1c** exhibits higher cellular bioluminescence production than that of LH_2 at lower concentrations (Figure 3A). The ability of **1c** to produce intense NIR bioluminescence, even at low concentrations, is similar to that of **1a**-HCl[20,21] and is beneficial because repetitive injections of large amounts of substrate, which is often required in animal imaging, can be avoided, decreasing the risk to animal health. As reported by Yeh et al.,[34] **1a**-HCl decreases the cell viability at higher concentrations (> 500 μM). On the other hand, **1c** does not affect the cell viability even at high concentrations (Figure 3B). Although toxicity of **1a**-HCl has not been observed in animal experiments so far,[21] the improvement of the solubility and cytotoxicity in **1c** can remove the potential problems of **1a**-HCl in animal experiments. Considerations on its toxicity are described in the Supporting Information (Section S3).

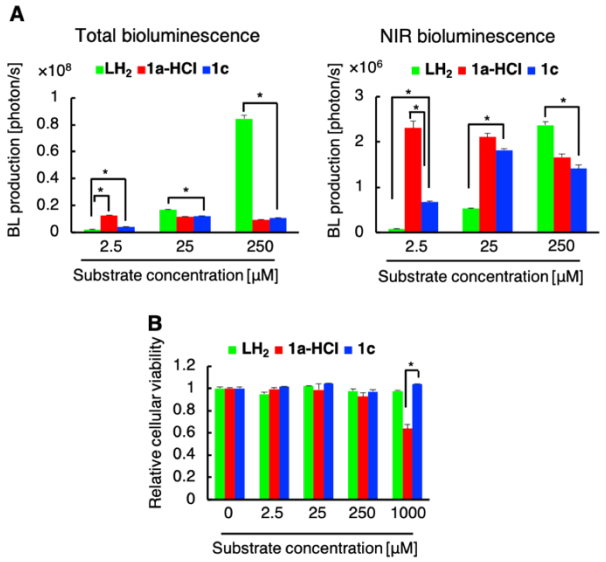

Figure 3. Cellular imaging. (**A**) Bioluminescence production in LLC/luc cells treated with different concentrations of the indicated substrates. Total (left) and NIR (right) bioluminescence were obtained with open filter or NIR filter (680±10 nm), respectively. n=3, *P<0.05. (**B**) Viability of LLC/luc cells treated with different concentrations of the indicated substrates. n=3, *P<0.05.

3.6. Animal imaging. The bioluminescence of **1c** are compared with that of LH_2 and **1a**-HCl in mouse tumor models. First, the bioluminescence signals from LH_2 and **1c** at subcutaneous tumors located near the body surface of mice were compared for the same dose. A slightly higher signal is detected from **1c**-injected mice compared to that from the LH_2-injected ones (Figure 4A). Thus, the benefit of using **1c** for bioluminescence imaging in subcutaneous tumors near the surface of the body is not significant. However, when we next compared the bioluminescence signals in lung metastasis, in which the targets are located deep inside the body, the NIR bioluminescence of **1c** improves the detection sensitivity for targets in deep tissues, exhibiting a six-fold increase in bioluminescence intensity compared to that of LH_2 (Figure 4B). In addition, **1c** exhibits a comparable sensitivity to that of **1a**-HCl in the imaging of lung metastases (Figure 4C). These results indicate that **1c** is a suitable substrate for bioluminescence imaging of deep tissues in small animals.

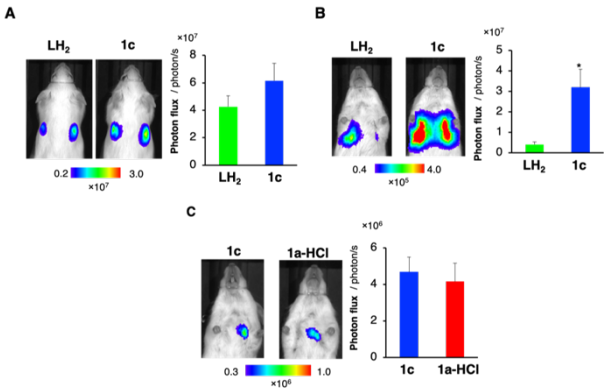

Figure 4. Animal imaging. (**A**) Bioluminescence production in subcutaneous LLC/luc tumors after injection with 33 mM LH_2 or **1c**. n = 6. (**B**) Bioluminescence production in LLC/luc lung metastases after injection with 33 mM LH_2 or **1c**. n = 6, *P < 0.05. (**C**) Bioluminescence production in LLC/luc lung metastases after injection with 33 mM **1c** or **1a**-HCl. n = 3.

4. Conclusion

We synthesized the *N*-aryl luciferin analogues **1b–d**, which were designed based on the NIR luciferin analogue **1a** (AkaLumine) for improved water solubility. As expected, **1b–d** exhibit higher solubility than that of **1a** in PBS. Specifically, **1d**

has the highest solubility among **1a–d**. Analogues **1b–d** exhibit moderate luminescence activities in L-L reactions with FLuc in KPB at pH 8.0. The λ_{BL} values for **1b–d** are presented in the red-NIR region, and **1c** exhibits a λ_{BL} value similar to that of **1a**. The λ_{BL} values of **1a–d** show a similar trend to that of the λ_{CL} values observed in DMF. DFT and TD-DFT calculation results indicate that these variations in the λ_{BL} and λ_{CL} values are largely determined by the electronic properties of the oxyluciferin analogues corresponding to **1a–d**. Because the water solubilities of **1b–d** are better than that of **1a**, the K_m values of **1b–d** are higher than that of **1a**. Interestingly, the pyridine-containing analogues **1b** and **1c** show higher relative V_{max} values than that of **1a**. Considering the observed c_{max}, λ_{BL}, and V_{max} values, **1c** was concluded to be the most suitable compound for cellular and animal imaging among **1b–d**. In fact, **1c** exhibits a higher NIR bioluminescence intensity than that of LH_2 at low concentration in cellular imaging of LLC/luc, being similar to that of **1a**-HCl. In the case of *in vivo* imaging of lung metastases located deep in the mouse bodies, the bioluminescence intensity of **1c** is six-fold higher than that of LH_2 and is equivalent to that of **1a**-HCl. These experimental data demonstrate that **1c** is of practical use for *in vivo* optical imaging of deep tissues.

Acknowledgement

The authors wish to thank Kurogane Kasei Co., Ltd., for providing AkaLumine and TokeOni (AkaLumine-HCl). The authors thank Daicel Chemical Industries, who analyzed the chirality of analogues **1b–d**. This work was supported in part by Grants-in-Aid for Scientific Research on Innovative Areas "Resonance Bio" (No. 15H05948) to S. A. M. and for Scientific Research (C) (No. 18K05075) to T. H. from Japan Society for the Promotion of Science, and Adaptable & Seamless Technology Transfer Program through Target-driven R&D (A-Step) (No. AS2614119N) to S. A. M. from the Japan Science and Technology Agency. We thank the Information Technology Center of UEC for technical assistance in DFT calculations.

Supporting Information

Supporting Information include on Speculation of toxicity in cell imaging for **1a**-HCl, DFT calculations of oxyluciferin forms of AkaLumine derivatives *oxy*-**1b–d** and the ^{1}H and ^{13}C NMR Spectrum data.

References

1 D. M. Close, T. Xu, G. S. Sayler, S. Ripp, *Sensors* **2011**, *11*, 180.

2 C. E. Badr, B. A. Tannous, *Trends Biotechnol.* **2011**, *29*, 624.

3 J. A. Prescher, C. H. Contag, *Curr. Opin. Chem. Biol.* **2010**, *14*, 80.

4 M. S. Evans, J. P. Chaurette, S. T. Adams, G. R. Reddy, M. a Paley, N. Aronin, J. a Prescher, S. C. Miller, *Nat. Methods* **2014**, *11*, 393.

5 C. H. Contag, M. H. Bachmann, *Annu. Rev. Biomed. Eng.* **2002**, *4*, 235.

6 T. Hirano, Y. Hasumi, K. Ohtsuka, S. Maki, H. Niwa, M. Yamaji, D. Hashizume, *J. Am. Chem. Soc.* **2009**, *131*, 2385.

7 B. R. Branchini, M. H. Murtiashaw, R. A. Magyar, N. C. Portier, M. C. Ruggiero, J. G. Stroh, *J. Am. Chem. Soc.* **2002**, *124*, 2112.

8 J.-B. Kim, K. Urban, E. Cochran, S. Lee, A. Ang, B. Rice, A. Bata, K. Campbell, R. Coffee, A. Gorodinsky, Z. Lu, H. Zhou, T. K. Kishimoto, P. Lassota, *PLoS One* **2010**, *5*, e9364.

9 R. Weissleder, *Nat. Biotechnol.* **2001**, *19*, 316.

10 R. Weissleder, V. Ntziachristos, *Nat. Med.* **2003**, *9*, 123.

11 S. T. Adams, S. C. Miller, *Curr. Opin. Chem. Biol.* **2014**, *21*, 112.

12 A. P. Jathoul, H. Grounds, J. C. Anderson, M. A. Pule, *Angew. Chemie* **2014**, *126*, 1.

13 B. R. Branchini, T. L. Southworth, D. M. Fontaine, D. Kohrt, C. M. Florentine, M. J. Grossel, *Sci. Rep.* **2018**, *8*, 1.

14 R. Kojima, H. Takakura, T. Ozawa, Y. Tada, T. Nagano, Y. Urano, *Angew. Chemie - Int. Ed.* **2013**, *52*, 1175.

15 M. P. Hall, C. C. Woodroofe, M. G. Wood, I. Que, M. Van'T Root, Y. Ridwan, C. Shi, T. A. Kirkland, L. P. Encell, K. V. Wood, C. Löwik, L. Mezzanotte, *Nat. Commun.* **2018**, *9*, 132.

16 S. Iwano, R. Obata, C. Miura, M. Kiyama, K. Hama, M. Nakamura, Y. Amano, S. Kojima, T. Hirano, S. Maki, H. Niwa, *Tetrahedron* **2013**, *69*, 3847.

17 C. Miura, M. Kiyama, S. Iwano, K. Ito, R. Obata, T. Hirano, S. Maki, H. Niwa, *Tetrahedron* **2013**, *69*, 9726.

18 M. Kiyama, S. Iwano, S. Otsuka, S. W. Lu, R. Obata, A. Miyawaki, T. Hirano, S. A. Maki, *Tetrahedron* **2017**, *74*, 652.

19 N. Kitada, T. Saitoh, Y. Ikeda, S. Iwano, R. Obata, H. Niwa, T. Hirano, A. Miyawaki, K. Suzuki, S. Nishiyama, S. A. Maki, *Tetrahedron Lett.* **2018**, *59*, 1087.

20 T. Kuchimaru, S. Iwano, M. Kiyama, S. Mitsumata, T. Kadonosono, H. Niwa, S. Maki, S. Kizaka-Kondoh, *Nat. Commun.* **2016**, *7*, 11856.

21 S. Iwano, M. Sugiyama, H. Hama, A. Watakabe, N. Hasegawa, T. Kuchimaru, K. Z. Tanaka, M. Takahashi, Y. Ishida, J. Hata, S. Shimozono, K. Namiki, T. Fukano, M. Kiyama, H. Okano, S. Kizaka-kondoh, T. J. Mchugh, T. Yamamori, H. Hioki, S. Maki, A. Miyawaki, *Science (80-.).* **2018**, *359*, 935.

22 N. A. Meanwell, *J. Med. Chem.* **2011**, *54*, 2529.

23 M. J. Frisch, G. W. Trucks, H. B. Schlegel, G. E. Scuseria, M. A. Robb, J. R. Cheeseman, G. Scalmani, V. Barone, B. Mennucci, G. A. Petersson, H. Nakatsuji, M. Caricato, X. Li, H. P. Hratchian, A. F. Izmaylov, J. Bloino, G. Zheng, J. L. Sonnenberg, M. Hada, M. Ehara, K. Toyota, R. Fukuda, J. Hasegawa, M. Ishida, T. Nakajima, Y. Honda, O. Kitao, H. Nakai, T. Vreven, J. A. Montgomery, Jr., J. E. Peralta, F. Ogliaro, M. Bearpark, J. J. Heyd, E. Brothers, K. N. Kudin, V. N. Staroverov, R. Kobayashi, J. Normand, K. Raghavachari, A. Rendell, J. C. Burant, S. S. Iyengar, J. Tomasi, M. Cossi, N. Rega, J. M. Millam, M. Klene, J. E. Knox, J. B. Cross, V. Bakken, C. Adamo, J. Jaramillo, R. Gomperts, R. E. Stratmann, O. Yazyev, A. J. Austin, R. Cammi, C. Pomelli, J. W. Ochterski, R. L. Martin, K. Morokuma, V. G.

Zakrzewski, G. A. Voth, P. Salvador, J. J. Dannenberg, S. Dapprich, A. D. Daniels, Ö. Farkas, J. B. Foresman, J. V. Ortiz, J. Cioslowski, D. J. Fox, *Gaussian 09, Revision D.01*, Gaussian, Inc., Wallingford, CT, **2004**.

24 A. D. Becke, *J. Chem. Phys.* **1993**, *98*, 5648.

25 C. Lee, W. Yang, R. G. Parr, *Phys. Rev. B* **1988**, *37*, 785.

26 P. J. Stephens, F. J. Devlin, C. F. Chabalowski, M. J. Frisch, *J. Phys. Chem.* **1994**, *98*, 11623.

27 R. Dennington, T. Keith, J. Millam, *GaussView, Version 5.*, **2009**.

28 D. Kato, D. Shirakawa, R. Polz, M. Maenaka, M. Takeo, S. Negoro, K. Niwa, *Photochem. Photobiol. Sci.* **2014**, *13*, 1640.

29 T. Tsubaki, T. Kadonosono, S. Sakurai, T. Shiozawa, T. Goto, S. Sakai, T. Kuchimaru, T. Sakamoto, G. Kondoh, S. Kizaka-kondoh, *Oncotarget* **2018**, *9*, 11209.

30 P. Naumov, Y. Ozawa, K. Ohkubo, S. Fukuzumi, *J. Am. Chem. Soc.* **2009**, *131*, 11590.

31 O. V. Maltsev, N. K. Nath, P. Naumov, L. Hintermann, *Angew. Chemie - Int. Ed.* **2014**, *53*, 847.

32 B. R. Branchini, T. L. Southworth, M. H. Murtiashaw, R. A. Magyar, S. A. Gonzalez, M. C. Ruggiero, J. G. Stroh, *Biochemistry* **2004**, *43*, 7255.

33 S. J. Strickler, R. A. Berg, *J. Chem. Phys.* **1962**, *37*, 814.

34 H. W. Yeh, O. Karmach, A. Ji, D. Carter, M. M. Martins-Green, H. W. Ai, *Nat. Methods* **2017**, *14*, 971.

Graphical Abstract

< Synthesis and luminescence properties of near-infrared *N*-heterocyclic luciferin analogues for *in vivo* optical imaging >

< Ryohei Saito, Takahiro Kuchimaru, Shoko Higashi, Shijia W. Lu, Masahiro Kiyama, Satoshi Iwano, Rika Obata, Takashi Hirano, Shinae Kizaka-Kondoh,* and Shojiro A. Maki*>

<Summary>
N-Heterocyclic derivatives (**1b–d**) of the near-infrared luciferin analogue, AkaLumine (**1a**) were synthesized. Among **1b–d**, **1c** (named as "seMpai") had higher solubility in PBS than **1a** and showed the same bioluminescence maximum as **1a**. In *in vivo* imaging experiments with mice, seMpai exhibited similar bioluminescence intensity to **1a**, supporting the usefulness of seMpai for near-infrared bioluminescence imaging of deep tissues.
<Diagram>